



Contents lists available at ScienceDirect

Defence Technology

journal homepage: [www.elsevier.com/locate/dt](http://www.elsevier.com/locate/dt)

# Liquid phase in-situ synthesis of LiF coated boron powder composite and performance study

Yang Xu <sup>a</sup>, Qing-zhong Cui <sup>a,\*</sup>, Cheng-wen Zhao <sup>b</sup>

<sup>a</sup> State Key Laboratory of Explosion Science and Technology, Beijing Institute of Technology, Beijing 100081, China

<sup>b</sup> Shanxi Jiangyang Chemical Factory, Shanxi 030000, China

## ARTICLE INFO

### Article history:

Received 2 July 2019

Received in revised form

31 July 2019

Accepted 19 August 2019

Available online xxx

### Keywords:

Boron

LiF

Coating

Thermal decomposition properties

Energy efficiency

## ABSTRACT

Among practical metal additives, boron (B) has a high volumetric heating value, making it a promising choice as a fuel additive. Although B can theoretically yield a large amount of energy upon complete combustion, its combustion is retarded by the initial presence of B oxide, which coats the surfaces of B particle. To improve the ignition and combustion properties of B powder, LiOH and NH<sub>4</sub>F were used as precursors to synthesize uniformly LiF-coated B composites (LiF-B) in situ. The LiF-B mixture was also prepared for comparison using a physical method. X-ray diffraction (XRD), Fourier-transform infrared (FTIR), scanning electron microscope (SEM), and energy-dispersive X-ray spectroscopy (EDS) were used to characterize the morphologies and compositions of the products. The thermal and combustion properties of the samples were characterized by thermal gravity-differential thermal gravity (TG-DTG), differential scanning calorimetry (DSC) and closed bomb experiment. The XRD, FTIR, SEM and EDS results demonstrated the successful preparation of the coated LiF-B sample. The TG-DTG and closed bomb experiment results indicated that the addition of LiF decreased the ignition temperature of B powder, and increasing its reaction efficiency. DSC results show that when LiF-B was added, the released heat of underwater explosive increased by 6727.2, 7280.4 and 3109.6 J/g at heating rates of 5, 10, and 15 °C/min, respectively. Moreover, LiF-B decreased the activation energy of secondary combustion reaction of explosive system as calculated through Kissinger's method by 28.9%, which indicated an excellent catalytic effect for the thermal decomposition of underwater explosive. The results reveal that LiF can improve the combustion efficiency of B powder, thereby increasing the total energy of explosives. The mechanical sensitivity increased slightly after adding LiF-B to the underwater explosive. Compared to the underwater explosive with added B, the mechanical sensitivity of the explosive with added LiF-B was significantly lower.

© 2019 The Authors. Production and hosting by Elsevier B.V. on behalf of China Ordnance Society. This is an open access article under the CC BY-NC-ND license (<http://creativecommons.org/licenses/by-nc-nd/4.0/>).

## 1. Introduction

Metal additives are common in solid rocket propellants and explosives due to their ability to increase energy density. In particular, B powder is attractive as a fuel or a fuel supplement in propellants and explosives because B has the highest gravimetric and volumetric heating values of any element [1,2]. Although B powder exhibits excellent performance, the ignition and combustion of B powder are limited by the formation of oxide film (B<sub>2</sub>O<sub>3</sub>)

with extremely high boiling temperature (2329 K) on the surfaces of B particles [3]. The high melting point of the oxide film makes the B powder difficult to ignite and results in low combustion efficiency, limiting the application of B powder in propellants and explosives [4]. Therefore, achieving the rapid and efficient combustion of B particles is critical for their application. To improve the combustion properties of B powder, it has been mixed with flammable metals to form composites or blends [5]. Liu et al. [6] studied the effects of B particle surface coatings, including LiF, Viton A, and silane coatings, on the combustion of solid propellants and found that the LiF-coated propellant exhibited the best overall behavior. The LiF and Viton A-coated propellants had the shortest and longest ignition times under the same heat flux, respectively. Xi Jian-fei et al. [7] experimentally investigated the effects of four metal

\* Corresponding author.

E-mail addresses: [xuyang0829bit@gmail.com](mailto:xuyang0829bit@gmail.com) (Y. Xu), [bit84021060@yeah.net](mailto:bit84021060@yeah.net) (Q.-z. Cui), [531520211@qq.com](mailto:531520211@qq.com) (C.-w. Zhao).

Peer review under responsibility of China Ordnance Society

<https://doi.org/10.1016/j.dt.2019.08.016>

2214-9147/© 2019 The Authors. Production and hosting by Elsevier B.V. on behalf of China Ordnance Society. This is an open access article under the CC BY-NC-ND license (<http://creativecommons.org/licenses/by-nc-nd/4.0/>).

hydrides on the burning characteristics of B powder and found that different metal hydrides promoted combustion to different extents. LiF was the most effective additive and shortened the ignition delay time of B powder by 34.1%. Moreover, LiF enhanced the combustion intensity of B powder by 117.6%. The other three metal hydrides ( $\text{CaH}_2$ ,  $\text{TiH}_2$ , and  $\text{ZrH}_2$ ) also promoted the burning of B powder. Liang Dao-lun et al. [8] studied the ignition and heterogeneous combustion of aluminum (Al) boride and a B–Al blend using a laser ignition testing system. The emission spectral intensity curves showed that the B–Al blend exhibited better ignition features than aluminum boride. However, the combustion intensity and self-sustaining combustion time of the B–Al blend were inferior to those of Al boride. These past studies indicate that the incorporation of metal materials or the coating B particles with metals fuels can promote the ignition and combustion of B powder. Furthermore, the superiority of LiF among additives in terms of its ability to improve the ignition and combustion properties of B particles was demonstrated both theoretically and experimentally in studies by King and Liu [9–11]. Although the potential advantages of LiF have been demonstrated, few systematic studies have been carried out on this material. At present, a large number of studies have used B in propellants to study the effects of B size and surface modifications on propellant performance. However, studies on the application of B powder in underwater explosives have rarely been reported. Many research [12–15] results have shown that the higher the detonation speed and pressure of the underwater explosion, the faster the attenuation of the shock wave pressure and the increase of the energy loss, which is not conducive to the damage of the target in the non-contact explosion. Therefore, in the process of water explosion and energy transfer, the damage effect of the non-contact explosion, depend on the detonation heat of the explosive. Compared to other common metal fuels, B powder has a higher mass calorific value (2.3 times that of magnesium and 1.9 times that of aluminum) [16,17]. Therefore, the addition of B powder to underwater explosives can effectively increase the detonation heat of the explosive, thereby increasing the energy level of the underwater explosives.

In this study, B powder was coated with LiF using a gas-liquid two-phase flow method that resulted in good coating uniformity. The coating optimized the combustion performance of B powder and improved the combustion efficiency. The modified B powder was applied in underwater explosives, and the superiority of the modified B powder in underwater explosives was verified.

## 2. Experimental

### 2.1. Materials

Amorphous boron was purchased from Tianyuan Chemical Industry Ltd. (Liaoning, China); Hexahydro-1,3,5-Trinitro-1,3,5-Triazine (RDX) was provided by Gansu Yinguang Chemical Industry Ltd. (Baiyin, China); Ammonium perchlorate (AP) was provided by Liming Chemical Ltd. (Luoyang, China); Al was provided by Dingli Technology Ltd. (Hunan, China); LiOH was provided by Oujin Industrial Ltd. (Shanghai, China);  $\text{NH}_4\text{F}$  was provided by Tianmao Industrial Ltd. (Xian, China).

### 2.2. Preparation of LiF-B composite

Since LiF is an inert substance, increasing the coating amount of LiF on B powder increases the time required for B powder to reach the ignition temperature. Therefore, the mass ratio of LiF coating to B powder is 1:10 [18]. LiF is typically coated on B powder using the traditional recrystallization method. In this method, the solvent in the suspension gradually evaporates, and the B particles deposit on

the bottom of the beaker, making it difficult to uniformly coat the B particles as the coating material crystallizes. Furthermore, crystallization mainly occurs via primary homogeneous nucleation, which results in the uneven coating of B particles.

In this study, LiF-B powder was prepared using an in-situ synthesis method. To uniformly coat the B particles, it was necessary to prevent particle coalescence. Therefore, a gas-liquid two-phase flow coating device was designed (Fig. 1). Under the action of ultrasonic waves and agitating paddles, the B powder was uniformly dispersed in LiOH solution.  $\text{NH}_4\text{F}$  solution was then impacted by a high-pressure gas stream, forming small mist droplets in the suspension. These droplets rapidly crystallized, resulting in the uniform deposition of LiF particles that adhered to the surfaces of the B powder particles. Finally, the complete coating of B powder with ultra-thin LiF was achieved.

The experimental process was as follows. First,  $\text{NH}_4\text{F}$  (weight: 1.4 g) was ultrasonically dispersed in 15 mL of deionized water to prepare an aqueous solution of  $\text{NH}_4\text{F}$ . Meanwhile, 10 g of amorphous B powder and 0.9 g of LiOH were dispersed in 39 mL of deionized water to prepare a B powder/LiOH aqueous solution. Next, the experimental device was turned on, and the  $\text{NH}_4\text{F}$  solution was introduced into the nozzle under the action of a vacuum pump at a flow rate of 30 mL/min. Finally, the two solutions collided with the high-pressure gas to form small droplets, and LiF rapidly crystallized from the atomized  $\text{NH}_4\text{F}$  solution and LiOH solution under high-speed stirring and ultrasonic treatment. The precipitated LiF formed a dense coating on the surface of B powder, resulting in the LiF-coated B composite (termed LiF-B).

Following the same procedure, pure LiF without B powder was prepared. For comparison, the LiF-B mixture was also prepared using a physical method.

### 2.3. Characterization

The morphology and size of the B powder and LiF-B were characterized though using a S-4800 scanning electron microscope (SEM) with EDS.

DX-2700 X-ray diffraction (XRD, Dandong Haoyuan Corporation, Liaoning, China) was used to analyze the crystalline phases of B, LiF and LiF-B composite at a voltage of 40 kV and a current of 30 mA using Cu-K $\alpha$  radiation at  $\lambda = 1.5418 \text{ \AA}$ .

Fourier transform infrared (FT-IR) spectra were characterized by a PerkinElmer Spectrum 100 to characterize B, LiF, LiF-B mixture and LiF-B. The sample was carried out in a KBr pellet by a MCT detector at a stand of distance of 5 m using a mid-IR super-continuum light source. It was measured in  $1600\text{--}600 \text{ cm}^{-1}$  wave number range with a  $4 \text{ cm}^{-1}$  resolution.

Thermal analysis of crystalline B, LiF-B mixture and LiF-B by German Netzsch STA449F3 thermobalance (TG and DTG). Temperature range: room temperature to  $1000 \text{ }^\circ\text{C}$ ; heating rate:  $10 \text{ }^\circ\text{C/}$

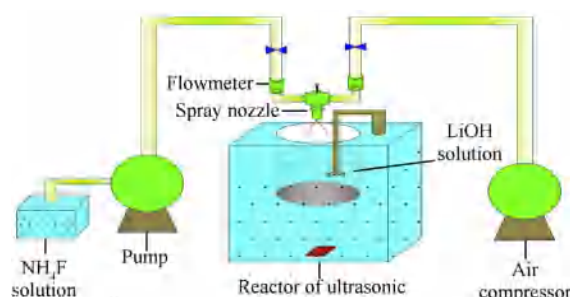


Fig. 1. Experimental diagram of LiF-B via gas-liquid two-phase flow method.

min. The experimental atmosphere was air, the flow rate was 40 mL/min, and the amount of sample was about 5 mg each time.

PBXN-111 (the most representative blasting warhead charge in the US Navy) as Formulation 1 (RDX 20%/AP 43%/Al 25%/HTPB 12%), replace 4% Al in PBXN-111 with 4% LiF-B as Formulation 2 (RDX 20%/AP 43%/Al 21%/LiF-B 4%/HTPB 12%). Two formulations were analyzed by the DSC-131 differential scanning calorimetry (DSC). The DSC conditions were as follows: sample mass, 0.7 mg; test temperature, 0–500 °C; heating rate, 5, 10, and 10 °C/min; nitrogen atmosphere, 30 mL/min.

The closed bomb experiment adopted the inner trigger type. The experimental conditions were: DYY-1 pressure sensor with a measuring range of 600 MPa; the volume of the closed bomb was 106 mL; the ignition charge was 10 g.

Impact and friction sensitivity tests were performed on Formulation 1, Formulation 2, and Formulation 3 (RDX 20%/AP 43%/Al 21%/B 4%/HTPB 12%). ERL type 12- drop hammer apparatus was used to conduct impact sensitivity test according to GJB-772A-97 standard method 601.1 [19]. Testing conditions consisted of drop weight of  $10.000 \pm 0.010$  kg, sample mass of  $50 \pm 1$  mg, relative humidity of 50%, and test number, 25. Test results were represented by explosion probability ( $P_1$ ). WM-1 pendulum friction apparatus was used to test the friction sensitivity based on the GJB-772A-97 standard method 602.1 [19]. Experimental conditions are shown as follows: pendulum weight, 1.5 kg; swaying angle, 90°; pressure, 3.92 MPa; sample mass,  $20 \pm 1$  mg; and test number, 25. Friction sensitivity is expressed as explosion probability ( $P_2$ ).

### 3. Results and discussion

#### 3.1. Morphological characterization

The morphologies of the amorphous B powder and LiF are shown in Fig. 2. As shown in Fig. 2(a), the amorphous B powder exhibited an irregular morphology, varied particle shapes, rough surfaces, many wrinkles and defects, and a large number of attached fine particles. The median diameter of B powder was approximately 7  $\mu\text{m}$ . Correspondingly, the LiF prepared by the gas-liquid two-phase flow method exhibited a spherical morphology with smooth particle surfaces and a particle size of approximately 1  $\mu\text{m}$ .

Fig. 3 shows low- and high-magnification SEM images of LiF-B and the physical LiF-B mixture. Fig. 3(a) and (b) show the typical morphologies of LiF-B at different magnifications. As shown in the SEM images, LiF particles were overlain on the surface of the B powder, forming agglomerates with the rough powder surfaces.

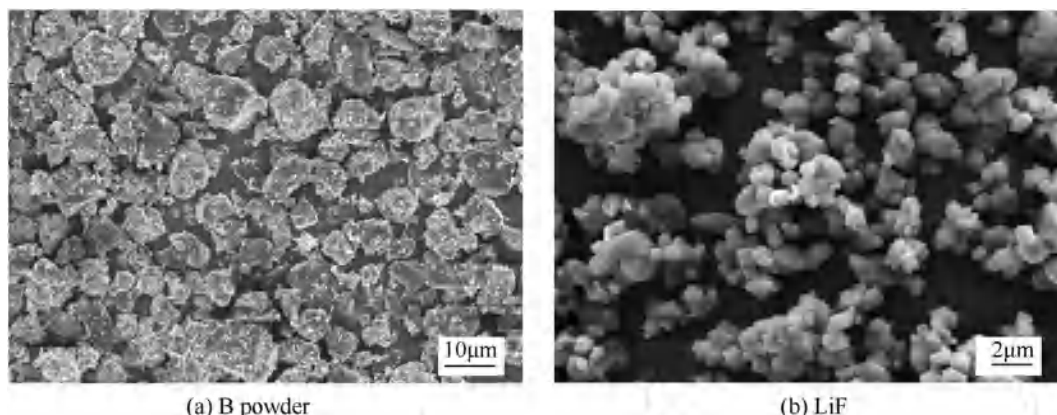


Fig. 2. SEM images of samples: (a) B powder, (b) LiF.

The median diameter of LiF-B was approximately 10  $\mu\text{m}$ , larger than that of the B powder. The corresponding elemental maps of B and F in LiF-B are shown in Fig. 3(c). The uniform distributions of F further confirm that LiF crystals were well distributed on the surface of B powder. The SEM images of the physical LiF-B mixture are shown in Fig. 3(e) and (f). The morphology of the physical LiF-B mixture was similar to that of LiF-B. However, the corresponding elemental maps for B and F show a poor combination of B and LiF in the physical LiF-B mixture (Fig. 3(g)). The SEM images show that B powder was successfully coated with LiF through the gas-liquid two-phase flow method. In order to further determine the element composition of the products, the EDS pattern of samples are shown in Fig. 3(d) and (h). Comparing the energy spectrum, it can be found that the characteristic peak of B almost disappears after the B powder was coated with LiF. It is indicated that LiF was well dispersed on the surface of B particles.

#### 3.2. XRD and FTIR analysis

The XRD patterns of B, LiF, LiF-B and LiF-B mixture are shown in Fig. 4(a). LiF displays three diffraction peaks at 39.0°, 45.0° and 65.5°, attributed to the (111), (200) and (220) crystal face (PDF Card 00-045-1460), indicating LiF was prepared successfully. The diffraction peaks of LiF-B are mainly resulting from B, with three additional diffraction peaks at 39.0°, 45.0° and 65.5°, indicating the presence of LiF. The FTIR spectra of LiF, B, LiF-B and LiF-B mixture are illustrated in Fig. 4(b). The infrared absorption peak of B powder at wavelength of  $550 \text{ cm}^{-1}$  can be identified, compared with the standard spectrum, which is the boron oxide ( $\text{B}_2\text{O}_3$ ) absorption peak, indicating the presence of  $\text{B}_2\text{O}_3$  on the surface of B powder. LiF has a characteristic absorption peak at a wavelength of  $1464 \text{ cm}^{-1}$ . The LiF-B mixture has two characteristic absorption peaks at wavelengths of  $1464 \text{ cm}^{-1}$  and  $550 \text{ cm}^{-1}$ . The infrared absorption peak at  $550 \text{ cm}^{-1}$  of B powder coated by LiF is obviously weakened. It is indicated that, the surface of B particle is covered by LiF.

#### 3.3. Thermal analysis

Fig. 5 shows the TG-DTG curves of the three samples. Table 1 shows the thermal characteristics of the three samples obtained from TG-DTG testing. Compared with B and LiF-B mixture, the ignition temperature ( $T_i$ ) of LiF-B was 113.9 °C and 75.2 °C lower, respectively. This demonstrates that the oxide film on the surface of B was removed by LiF, thereby reducing the ignition temperature of B and increasing the reactivity of B. The maximum weight gain rate

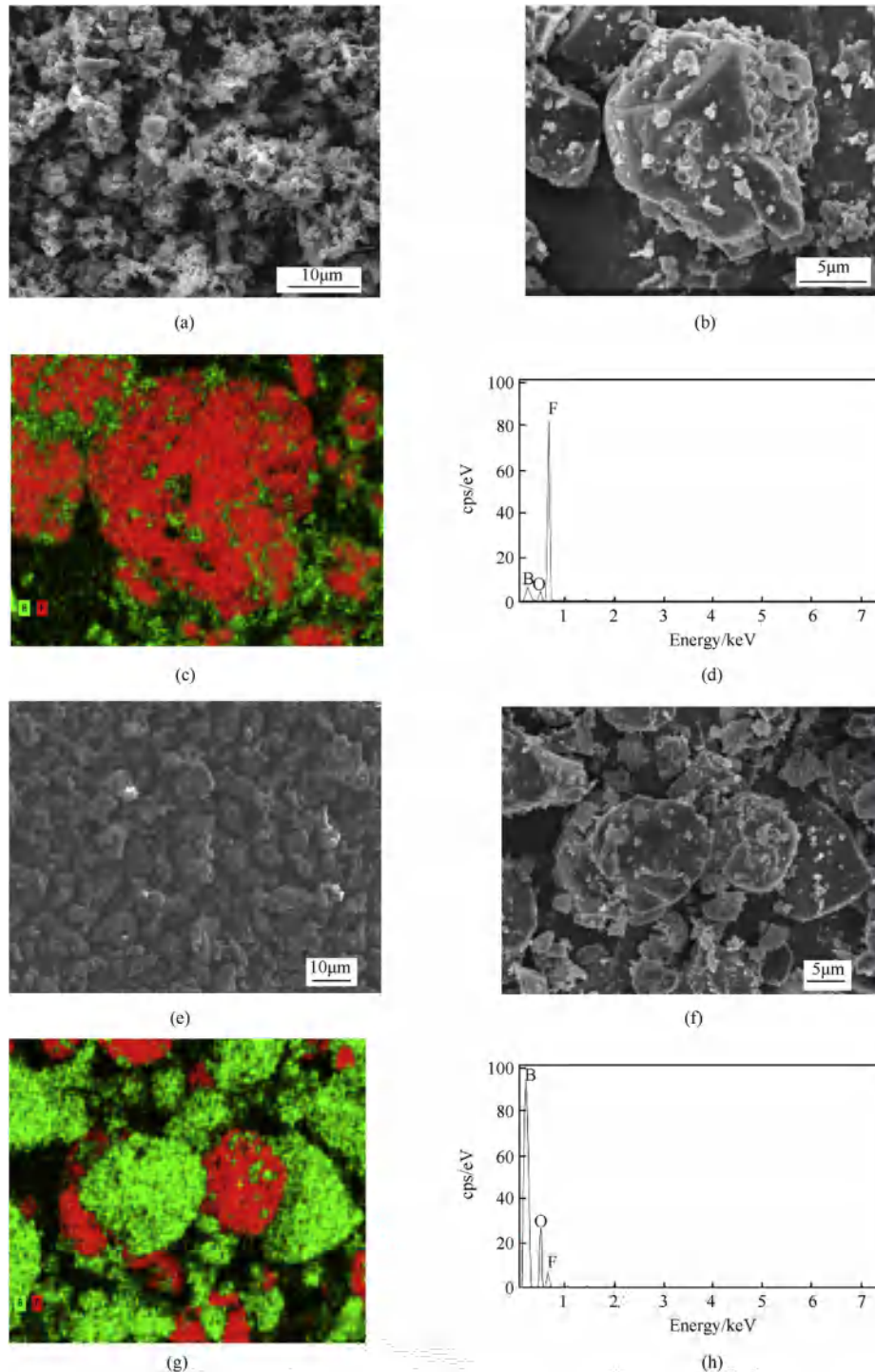


**Fig. 3.** (a, b, c) Low- and high-magnification SEM images of LiF-B and the corresponding elemental mapping image for boron (B) and fluorine (F); (d) EDS pattern of LiF-B particle; (e, f, g) Low- and high-magnification SEM images of LiF-B mixture and the corresponding elemental mapping images for boron (B) and fluorine (F); (h) EDS pattern of LiF-B mixture particle.

( $R_{\max}$ ) of Li-B was the largest among the three samples, which is attributed to the fact that LiF effectively removed the  $B_2O_3$  produced by the oxidation of B and increased the oxidation rate of B. The reaction efficiencies of B, LiF-B, and LiF-B mixture were calculated using Eq. (1) to be 56.9%, 64.5%, and 83.4%, respectively. Thus, coating B with LiF increased the reaction efficiency of B, resulting in a weight gain that was 65% and 46.7% higher than those of B and the LiF-B mixture, respectively.

The reaction efficiency is used to characterize the degree of reaction of sample, and can be expressed by Eq. (1).

$$\eta = \frac{(m_1 - m_0)/m_0}{16 \times 3 / (10.8 \times 2)} \times 100\% \quad (1)$$

where,  $\eta$  is reaction efficiency (%);  $m_0$  is initial reaction weight (mg);  $m_1$  is reaction end weight (mg).

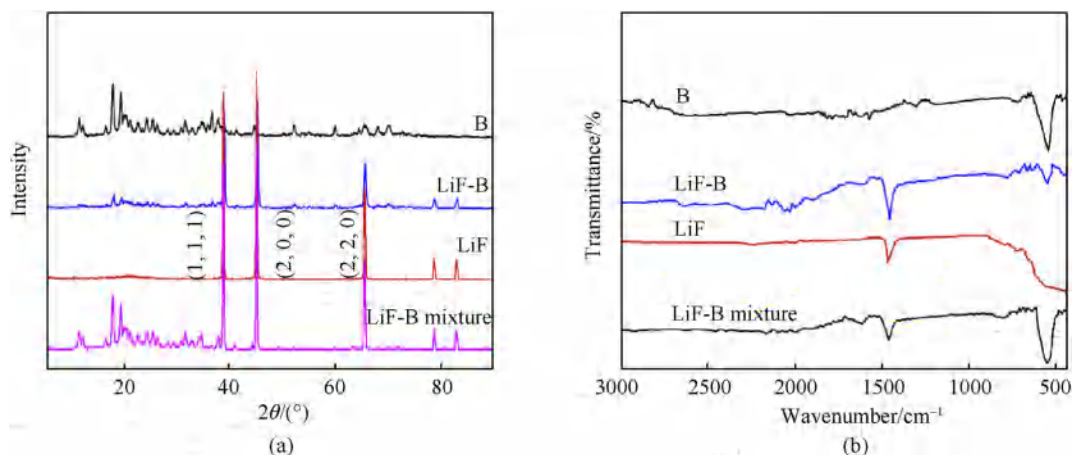


Fig. 4. XRD and FT-IR pattern of samples: (a) XRD patterns, (b) FT-IR spectra of sample.

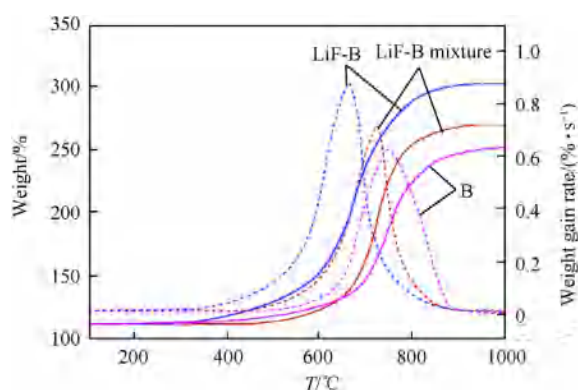


Fig. 5. TG-DTG curves of B, LiF-B mixture and LiF-B.

Table 1

The combustion characteristic parameters of samples.

samples	$T_i/^\circ\text{C}$	$R_{\max}/(\% \cdot \text{s}^{-1})$	$\eta/\%$	Weight gain/%
B	713.5	0.66	56.9	140.6
LiF-B mixture	674.8	0.72	64.5	158.9
LiF-B	599.6	0.87	83.4	205.6

The surface of the B powder particles was oxidized to  $\text{B}_2\text{O}_3$ , and the high melting point of  $\text{B}_2\text{O}_3$  (1862 °C) led to a decrease in the combustion efficiency of B.  $\text{B}_2\text{O}_3$  formed a layer of liquid oxide in the molten state that tightly coated the surfaces of the B particles. The  $\text{B}_2\text{O}_3$  molecules have a dense three-dimensional network structure and high viscosity; thus,  $\text{B}_2\text{O}_3$  decreased the volatility and hindered further contact between external oxygen and internal particles. The effective contact area between B and oxygen was reduced, and the reaction could not be completed. The reaction between LiF and  $\text{B}_2\text{O}_3$  formed a low-boiling-point complex, the dense three-dimensional network structure of  $\text{B}_2\text{O}_3$  was destroyed, the viscosity of the  $\text{B}_2\text{O}_3$  molten layer decreased, and the diffusion resistance of O in the  $\text{B}_2\text{O}_3$  molten layer was reduced, thereby accelerating the B/O reaction. The reaction can be written as follows:

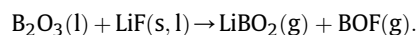


Fig. 6 is the reaction mechanism diagram of LiF-B.

Due to the high hardness of B, which is second only to diamond,

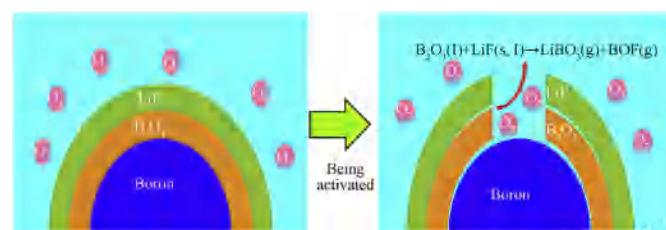


Fig. 6. Mechanism diagram of LiF-B oxidation reaction.

along with its brittle texture, adding a large amount of B to the explosive formulation can increase the sensitivity of the explosive. The safety test [19] indicated that the content of B in the formulation was less than 4%, which satisfies the requirements for ammunition use.

Fig. 7 shows the DSC curves of two formulations at heating rates of 5 °C/min, 10 °C/min and 15 °C/min. As shown in Fig. 7(a), the thermal decomposition of formulation 1 can be divided into four stages [19]: (1) the AP transition from orthorhombic to cubic at approximately 220 °C, as indicated by a significant endothermic peak in the DSC curve; (2) the partial low-temperature decomposition of AP at approximately 220 °C, as indicated by a weak exothermic peak; (3) the complete high-temperature decomposition of AP, as indicated by the relatively strong exothermic peak that appears following the low-temperature peak at temperatures ranging from 290 °C to 320 °C at different heating rates; (4) the rapid heat evolution associated with either the extremely fast

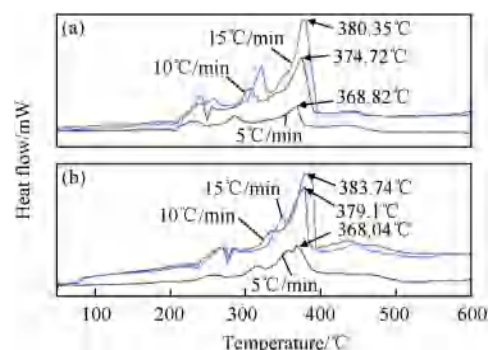


Fig. 7. DSC curves of different samples: (a) formulation 1, (b) formulation 2.

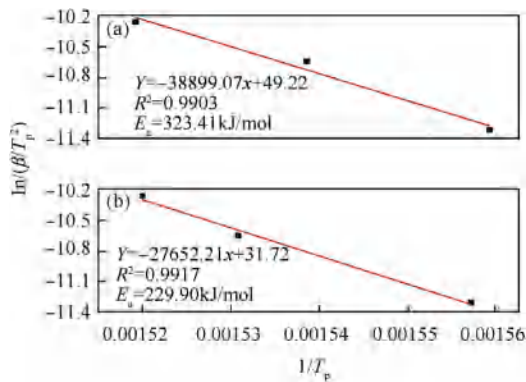


Fig. 8. Kissinger's plot of different samples: (a) formulation 1, (b) formulation 2.

decomposition kinetics or deflagration of RDX and the combustible agent Al, as indicated by the strong exothermic peak from 368 °C to 381 °C at different heating rates. The DSC curves of formulation 2 show a similar trend as those of formulation 1. By integrating the DSC curves, the released heats of the two formulations were obtained. At heating rates of 5 °C/min, 10 °C/min, and 15 °C/min, the released heats of formulation 2 were 6727.2, 7280.4, and 3109.6 J/g higher than those of formulation 1, respectively. Thus, the addition of LiF-B to the formulation effectively increased the heat release of the underwater explosive.

According to the three exothermic peak temperatures under different heating rates, the Kissinger method [20] can be used to calculate the thermal decomposition kinetics parameters of two formulas; as shown in Eq. (2).

$$\ln \frac{\beta_i}{T_{pi}^2} = \ln \frac{AR}{E_a} - \frac{E_a}{RT_{pi}} \quad (2)$$

where  $\beta_i$  is the heating rate (K/min);  $T_{pi}$  is the peak temperature of decomposition at  $\beta_i$  (K);  $A$  is the pre-exponential factor;  $E_a$  is the activation energy in (J/mol); and  $R$  is the universal gas constant (8.314 J/mol · K).

When the values of  $\ln(\beta_i/T_{pi}^2)$  are plotted against values of  $1/T_{pi}$ , a strong correlation is observed, which is shown in Fig. 8.

A strong correlation was observed when  $\ln(\beta_i/T_{pi}^2)$  was plotted against  $1/T_{pi}$ , as shown in Fig. 8. The activation energy  $E_a$  and the pre-exponential factor  $A$  were calculated from the slope ( $-E_a/R$ ) and

the intercept  $\ln(AR/E_a)$ , respectively. From Fig. 8, the  $E_a$  values of formulation 1 and formulation 2 were 323.41 and 229.90 kJ/mol, respectively. The  $E_a$  of formulation 2 was 93.51 kJ/mol lower than that of formulation 1, indicating that the delay time of the secondary reaction of the explosive was shortened, the reaction was more easily activated, and the exothermic reaction in the high-temperature zone resulted in a more complete energy release of the system and a higher energy utilization rate. From the perspective of chemical kinetics, formulation 2 had a higher energy release efficiency compared to formulation 1, and the secondary combustion reaction had a higher combustion heat output. Integration analysis indicated that the addition of LiF-B to the explosive improved the energy utilization rate of the combustible agent and catalyzed the secondary reaction of the explosive.

#### 3.4. Static burning properties analysis

To compare the combustion properties of the samples, the oxidation-reduction reaction system of AP and the samples were respectively prepared according to zero-oxygen-balance, and the pressure ( $P$ )–temperature ( $t$ ) curve was obtained in a closed bomb (Fig. 9(a)).

According to the test results, the pressure instantaneously reached the maximum value, and the maximum pressure of AP-B was the highest among the samples because of the addition of LiF, which did not participate in the reaction in the other two samples. The pressure curves of AP/LiF-B and AP/LiF-B mixture will rise again during the descent, because Li removes the  $B_2O_3$  from the B surface, and B can react with  $O_2$ . By integrating the  $P$ - $t$  curve, the working abilities of the three samples were obtained (Fig. 9(b)). The working abilities of the three samples were nearly the same within the first 0.2 s of the reaction. From 0.2 to 0.45 s, the working abilities of AP/B and AP/LiF-B mixture increase rapidly, because the LiF coating on the B surface hindered the reaction between AP and B. The working ability of the AP/LiF-B mixture was higher than that of AP/B, indicating that LiF had a catalytic effect on the reaction. From 0.45 s to the end of the reaction, the working ability of AP/LiF-B rapidly increased and reached 6.246 MPa · s after reaction completion; this value was 3.671 and 3.121 MPa · s higher than the maximum working abilities of AP/B and the AP/LiF-B mixture, respectively. The comparative analysis indicates that coating B with LiF significantly enhanced the working ability. Thus, coating with LiF improved the combustion efficiency of B and increased the completeness of combustion.

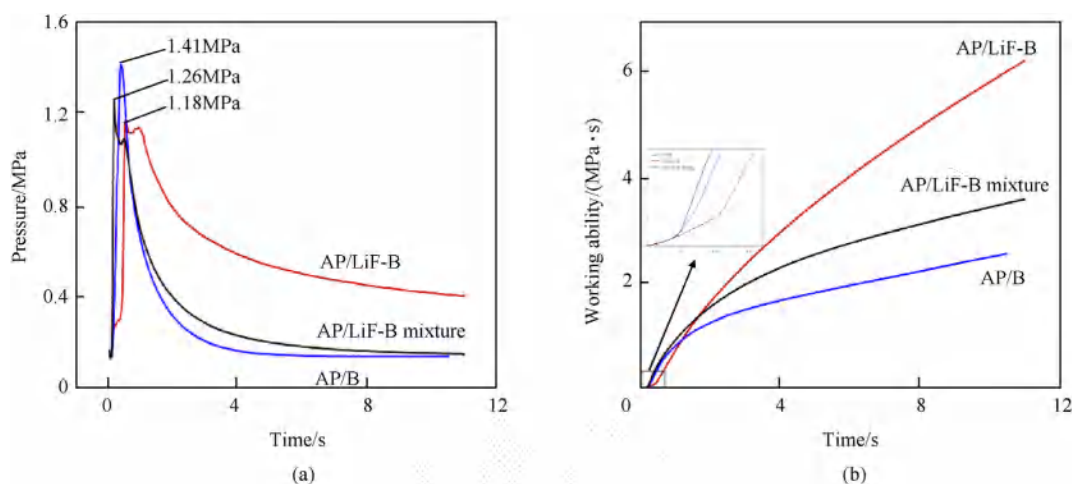


Fig. 9. The curve of closed-bomb test: (a) P-t curve, (b) Working ability.

**Table 2**  
Mechanical sensitivities of explosive samples.

samples	P <sub>1</sub> /%	P <sub>2</sub> /%
Formulation 1	24	28
Formulation 2	32	36
Formulation 3	64	100

### 3.5. Mechanical sensitivity characterization

As shown in Table 2, formulation 2 exhibited slightly higher impact and friction sensitivities compared to formulation 1. Although the LiF coating on the surface of B formed a protective layer, the hardness of boron is greater than that of Al, leading to a slight increase in mechanical sensitivity. However, the impact sensitivity and friction sensitivity of formulation 2 were 32% and 64% lower than those of formulation 3, respectively. This is because the LiF act as a shock absorber or diverter and transmits heat between B powder, RDX, and AP crystals under mechanical stimuli.

## 4. Conclusion

A new metal fuel, LiF–B, was successfully prepared using an in-situ method. XRD, FTIR, SEM, and EDS were used to confirm the compositions and morphologies of the samples, demonstrating the complete coating of B powder particles with ultra-thin LiF. TG-DTG analysis showed that LiF caused B to react easily under thermal stimulus; LiF decreased the ignition temperature of B by 16.0% and increased its reaction efficiency by 46.6%. DSC showed that the use of LiF–B in an underwater explosive effectively increased the heat release and decreased the activation energy of the secondary reaction. The use of LiF–B not only improved the energy utilization rate of the combustible agent it also catalyzed the secondary reaction of the explosive. The closed bomb experiment indicated that LiF improved the combustion efficiency of B and increased the completeness of combustion, thereby improving the working ability of the oxidation-reduction reaction system. Considering all the above results, the combustion performance of B powder can be effectively improved by coating with LiF through an in situ synthetic method, and LiF–B is suitable for use in underwater explosives.

## Acknowledgments

This work was supported by the National Natural Science

Foundation of China (Grant No.:3020050321328).

## References

- [1] Guo Y, Zhou X, Zhang W, Deng L, Du Y, Cheng S. Combustion characteristics of magnesium borides and their agglomerated particles. *Combust Flame* 2019;203:230–7.
- [2] Chintersingh K, Quang N, Schoenitz M, Dreizin EL. Combustion of boron particles in products of an air-acetylene flame. *Combust Flame* 2016;172:194–205.
- [3] Binnewies M, Milke E. Thermochemical data of elements and compounds, second, revised and extended edition. *Appl Math Mech* 2002;31:55–65.
- [4] Jung HJ, Sohn Y, Sung HG, Hyun HS, Shin WGWC. Physicochemical properties of ball milled boron particles: dry vs. wet ball milling process. *Powder Technol* 2015;269:548–53.
- [5] Chintersingh KL, Schoenitz M, Dreizin EL. Combustion of boron and boron–iron composite particles in different oxidizers(Article). *Combust Flame* 2018;192:44–58.
- [6] Liu Tai-Kang, Luh Song-Ping, Perng Huey-Cherng. Effect of boron particle surface coating on combustion of solid propellants for ducted rockets. *Propellants, Explos Pyrotech* 1991;16:156–66.
- [7] Liu JL, Xi JX, Yang WY, Hu YH, Zhang YZ, Wang YW, et al. Effect of magnesium on the burning characteristics of boron particles. *Acta Astronaut* 2014;96:89–96.
- [8] Liang D, Xiao R, Liu J, Wang Y. Ignition and heterogeneous combustion of aluminum boride and boron-aluminum blend. *Aero Sci Technol* 2019;84:1081–91.
- [9] Rosenband V, Natan B, Gany A. Ignition of boron particles coated by a thin titanium film. *J Propuls Power* 1995;11:1125–31.
- [10] Koroban VA, Burtsev YN, Alimov FR, Haustov AD, Dubovik VA, Teselkin VA. Thermal decomposition features of ammonium nitrate and its boron mixture under high pressures. *Propellants, Explos Pyrotech* 1994;19:307–10.
- [11] Pace KK, Jarymowycz TA, Yang V. Effect of magnesium-coated boron particles on burning characteristics of solid fuels in high-speed crossflows. *Int J Energetic Mater Chem Propuls* 1993;2:332–47.
- [12] Xiang D, Rong J, He X, Feng Z. Underwater explosion performance of RDX/AP-based aluminized explosives. *Cent Eur J Energ Mater* 2017;14:60–76.
- [13] Cao T, Zhou L, Zhang X, Wang J. Influence of booster size on the total energy of RBUL-1 explosive in underwater explosion. In: *IOP conference series:materials science and engineering*. China:Sanya; 2017.
- [14] Yin J, Yuan B, Zhou T, Li G, Ren X. The effect of nano-aluminum powder on the characteristic of RDX based aluminized explosives underwater close-filed explosion. In: *The 3rd international conference on mechatronics and mechanical engineering*. China:Shanghai; 2017.
- [15] Xu S, Chen Y, Chen X, Wu D, Liu D. Combustion heat of the Al/B powder and its application in metallized explosives in underwater explosions. *Combust Explos Shock Waves* 2016;52:342–9.
- [16] Yagodnikov DA. Experimental study of combustion of a cloud of boron particles in air. *Combust Explos Shock Waves* 2010;46:426–32.
- [17] Lima RJP, Dubois C, Mader O, Stowe R, Ringuette S. Boron nanoparticle-rich fuels for gas generators and propellants. *Int J Energetic Mater Chem Propuls* 2010;9:437–46.
- [18] Zhang Jiaoqiang, Zhang Qiongfang. Surface coating of superfine boron particles with lithium fluoride. *Chin J Explos Propellants* 2005;28:8–10.
- [19] Chinese national military STD GJB/772A-97. China: Peking; 1997.
- [20] Yang RT, Steinberg M. Reaction kinetics and differential thermal analysis. *J Phys Chem* 1976;9:965–8.